Hindawi Publishing Corporation
Journal of Chemistry
Volume 2013, Article ID 264832, 10 pages
http://dx.doi.org/10.1155/2013/264832

Research Article

Enhanced Catalyst Activity of WO_3 Using Polypyrrole as Support for Acidic Esterification of Glycerol with Acetic Acid

Khadijeh Beigom Ghoreishi,[1] Mohd Ambar Yarmo,[1] Norasikin Mohamad Nordin,[2] and Mohd Wahid Samsudin[1]

[1] *Faculty of Science and Technology, Universiti Kebangsaan Malaysia (UKM), 43600 Bangi, Selangor Darul Ehsan, Malaysia*
[2] *Department of Science, UTM SPACE, Universiti Teknologi Malaysia International Campus Jalan Semarak, 54100 Kuala Lumpur, Malaysia*

Correspondence should be addressed to Khadijeh Beigom Ghoreishi; khadijehbeigom@siswa.ukm.edu.my

Received 8 February 2013; Revised 14 July 2013; Accepted 16 July 2013

Academic Editor: Laura Pigani

A series of polypyrrole supported WO_3 were fabricated and characterized by FT-IR, XRD, XPS, BET, TGA, and FESEM-EDX. The activity of the catalysts was tested in glycerol esterification with acetic acid, and it found that WO_3-Ppy-20 (nanocomposite with 20% WO_3 loaded) showed the maximum catalyst activity with 98% and selectivity of 70% to triacetin at 110°C with a reaction duration of 10 h and also recorded the highest selectivity (75%) for acetylation of glycerol to monoacetin with about 59% conversion only. The highest acidity of WO_3-Ppy-20 is also confirmed using TPD-NH_3 analysis. The activity and selectivity to triacetin of the catalyst were enhanced by increasing WO_3 loading amount, resulting in 82% conversion for WO_3-Ppy-5 with about 32 and 50% selectivity to monoacetin and diacetin and about 18% selectivity to triacetin; in case of WO_3-Ppy-20, these amounts were changed to 5, 25, and 70% selectivity to monoacetin, diacetin, and triacetin, respectively with the conversion of 98%. TPD-NH_3 analysis found that polypyrrole supported WO_3 increases the catalyst acidity of WO_3. BET and FESEM analyses revealed that WO_3 particles were well dispersed with the smallest average size in nanocomposite compared to pure WO_3, which could contribute to the high activity of WO_3-Ppy catalyst for esterification of glycerol.

1. Introduction

Nanocomposites have provided new and exciting possibilities in the field of materials science [1–3]. Conducting polymer-based composites are more and more intensively studied since the end of the 1990s. These inorganic-organic hybrids form a promising class of new materials, owing to the advantageous properties of the polymer matrix and the embedded inorganic particles. The combinations often lead to synergistic effects, resulting in enhanced properties, making these materials applicable in various fields such as fuel cell [4], catalysis [5, 6], and sensors [7]. Metallic nanoparticles can be introduced in the polymer matrix either by chemical [8] or electrochemical methods [9–11]. Although various metals have already been introduced into the conductive polymer matrix by electrochemical deposition for applications in electrocatalytic reaction, very few papers report the use of conducting polymers as a support of novel metals for applications in catalysis [12, 13]. Although conducting polymers are commonly used as a support for metallic catalysts, neither the exact role of the polymer nor the relative contribution of each component to the enhancement of the catalytic activity of the composite is fully understood yet. The incorporation of metallic or semiconducting nanoparticles in conducting polymers such as polyaniline (PANI) is of interest because of the strong electronic interaction between the nanoparticles and the polymer matrix [14, 15]. Metal nanoparticles incorporated into conducting polymers are also known to enhance the conductivity of the polymers. Using an oxide support such as SiO_2, Al_2O_3, TiO_2, and ZrO_2 to improve the catalytic

activity of the active metal oxide phase is an old, well-known strategy. During the last decade, a significant development in catalysis research had been focused on improving the activity and selectivity of supported metal oxide catalysis by improving the properties of the support oxide material. This is generally known as the metal oxide support effect [16]. The conducting polymers (polyaniline, polypyrrole, ...) seem to be a convenient support for the active phase of catalyst [17, 18]. This kind of matrix is useful especially for oxidative-reductive catalysts, in which the catalytic process involves an exchange of electrons between reactants/products and catalyst [19]. To maximize the excellent properties of polymer-metal nanocomposites, homogeneous dispersion of metal nanoparticles in the polymer matrix is required. This is a key challenge due to their easy aggregation arising from their high surface free energy [20]. In the design of nanocomposites, one must consider the properties of the polymer matrix as well as the stability of the nanoparticles and more importantly the prevention of particle aggregation [21].

In the present work, we aimed to study the esterification of glycerol with acetic acid, as this reaction is a decent alternative for converting excess glycerol, which is obtained from biodiesel production process, to value-added chemical acetins (i.e., monoacetin, diacetin, and triacetin), which have significant applications in cryogenic manufacture, plastics, fuel additives, and many uses in cosmetic, food, and pharmaceutical industries. They are also used in the manufacture of explosives, plasticizers, softening, lubricants, and emulsifying agents uses and as a raw material in the production of biodegradable polyesters [22–27].

Typically, the esterification reaction is an acid-catalysed process. Many kinds of solid acids have been found: their acidic properties, their catalysis, and the structure of acid site have been elucidated, and those results have been reviewed by several workers [28]. Acid catalysis plays a key role in many important reactions of the chemical and petroleum industries and in environmentally benign chemical processes [29]. Liquid super acids based on sulphuric acid, which are efficient and selective at room temperature, are not suitable for industrial processes due to separation problems tied with environmental protection [30]. Among solid acid catalysts, tungsten oxide-based materials comprise an interesting class of acid solids, first reported as a strongly acidic system by Hino and Arata [31]. WO_3-ZrO_2, catalyst was also reported to be active for transesterification and esterification reactions under specific conditions [32, 33]. Thus, acid catalyst could play an important role in the glycerol dehydration stage as well as working under milder reaction conditions that might increase the conversion and selectivity. The use of two support materials could provide an alternative method to enhance the acidic condition and also the activities of the catalyst. To the best of our knowledge and with respect to what is extended above about the effective role of polypyrrole on enhancing the acidity of the metal oxide, we describe the preparation of a series of catalysts based on WO_3 supported on polypyrrole.

In relation to what is referred to above, we investigated the catalytic behaviour of WO_3/Ppy composite in glycerol esterification with acetic acid. Micelle method was considered to synthesize the nanocomposite in order to achieve the maximum catalytic properties by making well-dispersed particles. In this paper, the influence of parameters such as temperature and time, catalyst amount, and WO_3 loading percentage on the acid properties has been studied; finally, the catalytic behaviour in the esterification of glycerol with acetic acid has been evaluated.

2. Experimental

2.1. Materials and Preparation of WO_3 Nanoparticles (NPs). For preparation of WO_3 NPs, hexadecyl trimethyl ammonium bromide (CTAB) (purity approx. 99%) was purchased from Sigma. Tungsten(VI) chloride (WCl_6) (purity 99%) and ammonia solution (25% v/v) were purchased from Aldrich and BDH, respectively. Deionized and double distilled water was used for micelle and solution preparation. All the chemicals and solvents were used as received without further purifications. Firstly, the 0.05 M of CTAB solution was prepared. After getting the clear solution, 10 mL of ammonia solution (25 wt%) was added to the CTAB solutions while stirring. After getting a homogenous solution, 0.117 mol of WCl_6 1000 mL^{-1} of CTAB solution was added with vigorous stirring. After stirring for 4 h, the product was aged at ambient temperature for 72 h. The final product was filtered, washed with deionized water and absolute ethanol in order to remove surfactant, residual reactants, and by products, and then calcinated at 500°C for 2 h.

2.2. Polypyrrole and WO_3-Ppy PNCs (Polymer Nanocomposites) Preparation. Pyrrole (C_4H_5N), ammonium persulfate (APS, $[(NH_4)_2S_2O_8]$, and *p*-toluenesulfonic acid (PTSA, $C_7H_8O_3S$) were all purchased from Sigma Aldrich. For polypyrrole synthesis, the solution of PTSA and APS with a fixed ratio of 60 mmol : 36 mmol in 400 mL deionized water was mixed and sonicated for 1 h in an ice-water bath. Pyrrole solution is added to the mixture (74 mmol in 100 mL deionized water, molar ratio of APS : PTSA : pyrrole = 0.81 : 0.49 : 1). The obtained solution turns to dark green, indicating the polymerization of pyrrole. The resultant precipitant is washed with deionized water and methanol to remove any possible oligomers. The obtained powders are dried completely at 50°C. For preparation of nanocomposite, the prepared WO_3 NPs were initially mixed with the solution of PTSA and APS with a fixed ratio of 60 mmol : 36 mmol in 400 mL deionized water, followed by 1 h sonication in an ice-water bath. The pyrrole solution (74 mmol in 100 mL deionized water, molar ratio of APS : PTSA : pyrrole = 0.81 : 0.49 : 1) was mixed with the above WO_3 NPs suspended solution at 0°C and then sonicated for an additional 1 h in an ice-water bath for further polymerization. The resultant solution turned greenish immediately and then black, indicating the polymerization of pyrrole. The product was precipitated naturally and washed with deionized water until the supernatant was transparent. The clear supernatant was then decanted to remove any unreacted PTSA and APS. The precipitant was washed with methanol to remove any possible oligomers. The obtained

powders were dried completely at 50°C. Pure PPy, WO_3-PPy nanocomposites, with a particle loading of 5, 10, 15, and 20 wt%, were fabricated.

2.3. Catalyst Characterizations. The surface area of the supported WO_3 catalyst was measured using the BET method (N_2 adsorption) with a Gemini apparatus (Micromeritics 2010 Instrument Corporation). The morphology and microstructure data for the samples were obtained from FESEM using LEO 1450 VP equipped with energy dispersive X-ray detector (EDX). All the samples were analysed in a high vacuum at 20 kV. The phase structures of the catalysts were determined by an X-ray diffraction (XRD) using Bruker AXS D8 Advance diffractometer with Cu Kα (λ = 0.15406 nm) at an angle of 2θ = 20–80°. The sample (2.0 g) was grinded, and the fine powder was pressed and placed on the sample holder. The X-ray photoelectron spectrum (XPS) data of the as-prepared samples was obtained using an XPS type Ultra from Kratos. The samples were analysed at 3×10^{-9} mbar using C1s line at 284.6 eV from adventitious carbon as a reference for the binding energies. The acidity properties of the catalytic materials were measured by a temperature-programmed desorption of ammonia. These experiments were performed in a gas flow system equipped with a thermal conductivity detector (TCD). Prior to monitoring of the TPD-NH_3 profiles, the samples (50–60 mg) were placed in a U-shaped quartz reactor and heated in a helium flow at 150°C for 30 min. After a cooling temperature of 70°C, the samples were exposed to ammonia and flushed with 50 mL/min helium for 60 min. The TPD measurement was carried out with a heating rate of 10°C/min up to 600°C under flowing helium (50 mL/min). Desorption of ammonia was monitored by a TCD. The reduction characteristics of the catalysts were studied by a temperature-programmed reduction (TPR) using the same apparatus and pretreatment method for the TPD measurements. After pretreatment, the temperature was raised from 30°C to 1000°C at a rate of 10°C/min in a 10% H_2/He flow (30 cm^3/min).

2.4. Catalyst Activity Measurements. The esterification reactions were carried out under a vacuum in the temperature range 50–110°C with acetic acid to glycerol mole ratio of 6 in a stirred batch reactor and reflux condition. A Dean-Stark trap was attached to the 50 mL round bottom flask, in order to extract the water that deactivates the catalysts and causes reversibility of the esterification reaction. In a typical experiment, 0.4 g of the catalyst was loaded into the well miscible solution of reactants in the container. The stirring speed was maintained at 500 rpm. After cooling, the catalyst was separated from the solution mixture by centrifugation. These products were analysed by a gas chromatography using GC-Hewlett Packard Model 6890N equipped with a flame ionization detector (FID) and a capillary column of HP-5 (with 30 m length, 0.25 mm ID, and 0.25 μm of film thickness). The GC injection port and the detector temperature were set at 240 and 260°C, respectively. The initial column temperature was set at 70°C for 2 min and programmed from 70°C to 150°C for 1.5 min at the rate of 45°C · min^{-1}, from 150°C to 180°C at the rate of 8°C · min^{-1}, and from 180 to 240°C at the rate of 35°C · min^{-1}. The peak areas were used for quantification and the calibration curve. For every analysis, we transferred the weighted amount of the collected sample and 1 mL of 1-hexanol solution (5000 mg · L^{-1}) as an internal standard to a volumetric flask and made up to 10 mL with absolute ethanol [34].

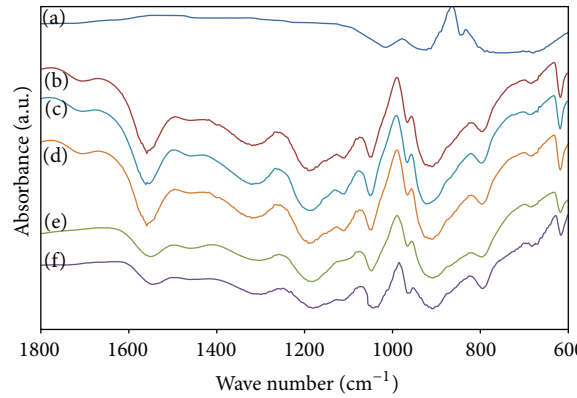

FIGURE 1: FT-IR spectra of WO_3-Ppy PNCs with particle loadings of (a) pure WO_3, (b) 5, (c) 10, (d) 15, (e) 20 wt%, and (f) pure Ppy, respectively.

3. Results and Discussion

Figure 1 shows the FT-IR spectra of the pure Ppy and WO_3-Ppy PNCs. Pure Ppy and the nanocomposites show the same peak locations at 1523 and 1428 cm^{-1}, which are assigned to C=C and C–N stretching, respectively. The peak near 1129 cm^{-1} corresponds to the breathing vibration of the pyrrole ring, and the peaks at 1271, 1003, and 702 cm^{-1} can be attributed to the C–H in-plane and out-of-plane deformation vibrations, respectively. The small band at 958 cm^{-1} is due to the C–C out-of-phase deformation vibration. It can be observed that the spectra of the PNCs have no obvious difference compared to that of pure Ppy. The slight peak shifts of the PNCs are as a result of the interaction between the NPs and the polymer matrix [35]

Figure 2 illustrates the XRD patterns of the WO_3 NPs and Pure Ppy and their corresponding PNCs. The XRD patterns of WO_3 NPs (Figure 2(a)) match well to the previous reported monoclinic structure [35], and the strong intensity of the diffraction peaks indicates a highly crystalline structure. According to the XRD measurement, all WO_3-Ppy catalysts contain monoclinic phase. The diffraction peaks (2θ) at 23.1, 23.6, 24.4, 26.6, 28.9, 33.3, 34.2, and 36.2° are attributed to the (002), (020), (200), (120), (112), (022), (202), and (212) planes of the monoclinic WO_3, respectively. Figures 2(b)–2(e) show the XRD patterns of the PNCs with different particle loadings. No additional peaks are observed for the PNCs as compared to those of the pure particles. However, a broad peak of the semicrystalline Ppy around 2θ = 21–25° is observed in the previous reports [36]. In this work, it is reasonable to consider that the broad peak of Ppy is

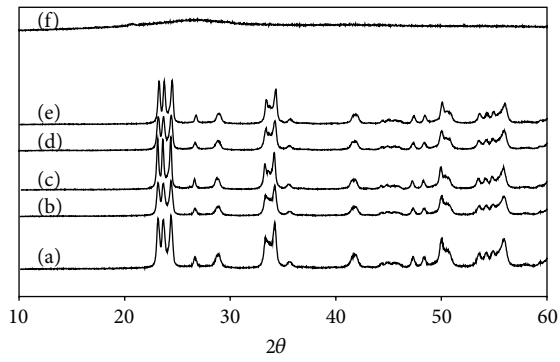

Figure 2: XRD patterns of (a) WO_3 NPs and WO_3-Ppy. PNCs with particle loadings of (b) 5, (c) 10, (d) 15, (e) 20 wt%, and (f) pure Ppy, respectively.

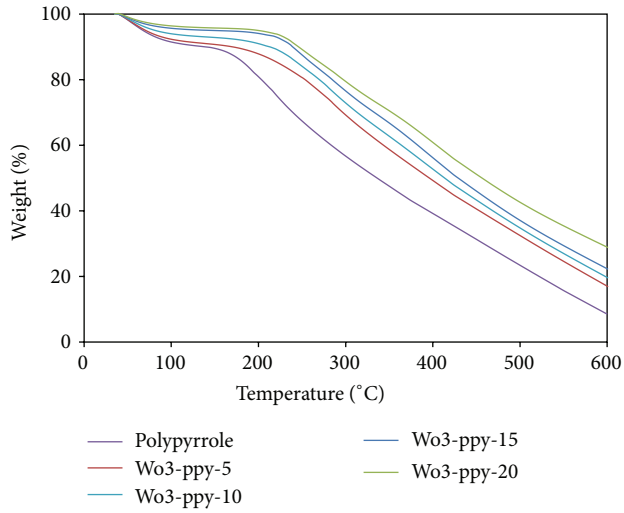

Figure 3: Thermogravimetric curves of the pure PPy and WO_3-Ppy PNCs.

overlapped by the large diffraction intensities of the (002), (020), and (200) crystal faces of WO_3 NPs. Compared to the pure particles, the decrease in the intensities of the WO_3 peaks in the PNCs (Figures 2(b)–2(e)) suggests that the WO_3 NPs are highly dispersed in the Ppy matrix, while the broadness of the peaks remains the same, moreover suggesting a uniform dispersion of the nanoparticles without serious agglomeration, as revealed by the FESEM observation in Figure 7 [35].

Figure 3 shows the thermal stability of pure PPy and its WO_3-Ppy PNCs with a particle loading of 5, 10, 15, and 20 wt%, respectively. All the samples show two distinct weight loss stages. The first stage, which corresponds to 5–10% weight loss from 25 to 260°C, is due to the evaporation of moisture and solvent residue in the samples. The major weight loss above 260°C is attributed to the degradation of PPy. With the addition of the WO_3 NPs, the degradation temperature (10% weight loss) of Ppy (231°C) increases to 269.4, 275.0, 277.0, 282.9, and 297.0°C for the PNCs filled with a particle loading of 5, 10, 15, and 20 wt%, respectively. The enhanced

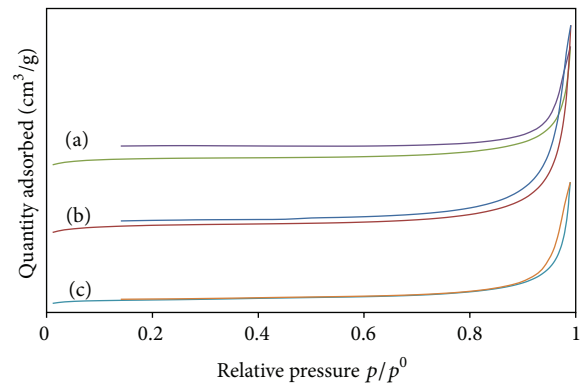

Figure 4: N_2 adsorption/desorption isotherms of (a) WO_3-Ppy-20 nanocomposite, (b) Pure Ppy, and (c) WO_3 NPs.

thermal stability of the nanocomposites is attributed to the more compact structure of Ppy induced by the addition of the WO_3 nanofillers, which can also be observed in the FESEM investigation.

The surface area of the pure Ppy, WO_3 NPs, and WO_3-Ppy nanocomposite was measured using the Brunauer-Emmett-Teller (BET) method (N_2 adsorption) with a Gemini apparatus (Micromeritics 2010 Instrument Corporation), and the typical BET diagrams are depicted in Figure 4. WO_3-Ppy-20 nanocomposite isotherm was considered, as this species exhibited the most acidic performance among other loading nanocomposite catalysts, which is obtained from NH_3-TPD analysis. The isotherms were identified as type IV isotherms with H_3 hysteresis loop which is the indicator of mesoporous structure. The details of BET specific surface area and pore size, along with total acidity of pure Ppy, WO_3, and WO_3-Ppy nanocomposite, are listed in Table 1. The surface area of WO_3 loaded polypyrrole samples is higher than that of pure polypyrrole and WO_3. The results indicated that the addition of WO_3 slightly increased the specific surface area of the polypyrrole. The highest surface area was observed from a sample with WO_3-Ppy-20. The increase of WO_3 loading decreased the pore size on average. These results highlighted the mesoporous structure of the nanocomposite, which makes an efficient interaction between the surface of the compound and the nanocomposite catalyst.

The temperature programmed reduction was used to study the reducibility of the catalyst. According to the literature [37], pure WO_3 exhibits three reduction peaks, namely, a shoulder at 540°C ($WO_3 \rightarrow W_{20}O_{58}$), a sharp peak at 775°C ($W_{20}O_{58} \rightarrow WO_2$), and a peak at higher temperature ($WO_2 \rightarrow W$). Figure 5(a) shows the three main peaks of WO_3, indicating reduction of WO_3 species to metallic W. To understand the promotion effect of polypyrrole, the H_2-TPR of WO_3-Ppy nanocomposite is considered. In terms of WO_3-Ppy nanocomposite, all these peaks are observed, and also an additional peak is exhibited around 200°C due to some reduction on the support. The profile of nanocomposite indicates that all three reduction temperatures in WO_3 were decreased while their peak areas were increased in the presence of polypyrrole. Results revealed that the mobility

Table 1: Acidic properties of the samples obtained from TPD of ammonia.

Sample	S_{BET} [a]	D_P [b]	Temperature at maximum (°C)	Total acidity (μmol·g^{-1})
WO_3	1.38	28.50	350	316
WO_3-Ppy-5	9.01	10.73	130, 223, 390	535
WO_3-Ppy-10	9.35	10.87	132, 226, 384	659
WO_3-Ppy-15	10.84	10.21	134, 227, 407	754
WO_3-Ppy-20	11.17	10.16	137, 230, 370	1250
Ppy	10.53	15.29	127, 183, 211	647

[a]Multipoint BET surface area (m^2 g^{-1}).
[b]Pore Size (nm).

and availability of O_2 in nanocomposite are higher than WO_3. These phenomena might be related to the electron pair of N atoms in polypyrrole which acts as the donor of electron to WO_3, increasing the electron density on W. In other words, it is concluded that polypyrrole improves the redox properties of W^{6+} making WO_3-Ppy nanocomposite a suitable redox catalyst.

3.1. Acidity Studies Using TPD-NH_3. The acidity of the catalysts was quantified by the integration of desorption curves for TPD-NH_3. The areas under the curves were considered as being proportional to the number of moles of gas desorbed from the surface. The number of moles of NH_3 per weight of active phase is hereafter referred to as $n$$NH_3$. The maximum temperature on the curves was designated as T_{max}. Desorption peaks in maximum temperature ranges of 180–250, 280–330, and 380–500°C are normally attributed to NH_3 chemisorbed on weak, medium, and strong acid sites, respectively [38]. The TPD profiles corresponded to desorption of NH_3 from the surface of catalysts which were summarized in Figure 6, and the values of T_{max} and $n$$NH_3$ were shown in Table 1. The NH_3-TPD technology was usually used to measure the acidic properties of supports. The acidity strength was characterized by the temperature of desorption peak, while the number of acidic sites was measured by the amount of NH_3 desorbed. The NH_3-TPD profiles of the WO_3-Ppy nanocomposite catalyst with different loading ratios are shown in Figure 7. One broad peak was centred at 340°C for WO_3 [39], while three consequent peaks appeared in the temperature range of 100 to 250°C for polypyrrole. In the case of WO_3-Ppy nanocomposites, all species with 5, 10, 15, and 20% loadings exhibited a shoulder at around 135°C in the weak acid site, followed by two sequential peaks at about 250 and 400°C, which designated the medium and strong acid sites. It is observed that the intensity of the desorption peak decreased in relation to the increase in amount of WO_3 loading. This resulted in WO_3-Ppy-20 indicating the higher NH_3 desorption among all species by 1252 $\mu mol \cdot g^{-1}$ total acidity, which is in accordance with the fact that the amount of acid sites increased gradually as the WO_3 loading increased. As the glycerol acetylation is an acid catalysed reaction, the conversion of glycerol increased with an increasing amount of acid site, confirming that WO_3-Ppy-20 shows the most acidic properties among all species.

The morphologies of the prepared WO_3-Ppy nanocomposite and pure polypyrrole are shown in Figure 7. Both

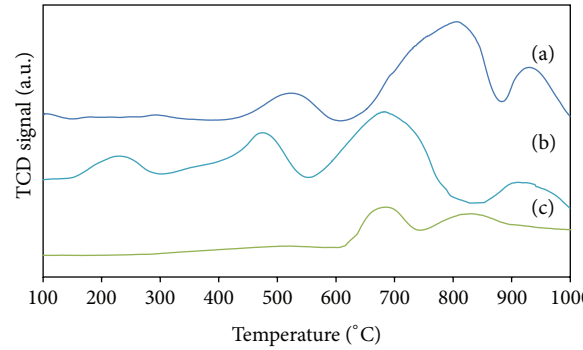

Figure 5: H_2-TPR profiles of (a) WO_3 NPs, (b) WO_3-Ppy nanocomposite, and (c) Pure Ppy.

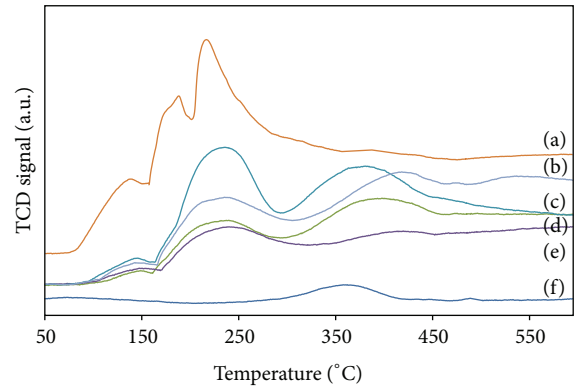

Figure 6: NH_3-TPD profiles of (a) pure Ppy and WO_3-Ppy with particle loadings of (b) 20, (c) 15, (d) 10, (e) 5 wt%, and (f) WO_3 NPs, respectively.

pure Ppy and its nanocomposite present a specific structure with a fairly uniform size distribution. The nanocomposite exhibits a highly mesoporous structure, which leads to the interest in its application as a catalyst [40]. This structure is totally incompatible with the results obtained from the N_2-adsorption/desorption isotherms. The pure PPy particles are observed to be relatively loosely packed as compared to the nanocomposite. For the nanocomposite filled with WO_3 nanoparticle, the particles are closely packed, and no bare nanoparticles are observed, which confirms that the micelle technique produced a well-dispersed nanoparticle.

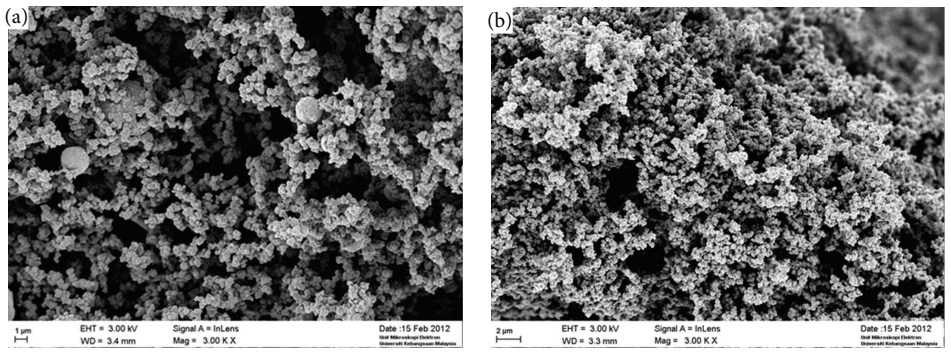

(a) (b)

Figure 7: FESEM images of (a) pure Ppy and (b) WO_3-Ppy nanocomposite.

Micelle does not only provide a favourable site for the growth of the particulate assemblies but also influences the formation progress including nucleation, growth, coagulation, and flocculation. The surfactant-assisted method is an effective process to prepare size controllable nanocrystals, which is a simple, convenient, and low-cost process [41].

To determine surface composition and the chemical state of prepared samples, the XPS measurements were done, and results are depicted in Figure 8. The C1s photoelectron peak with binding energy of 284.6 eV was used as a reference to correct any charging effect. There was not any impurity peak observed due to thorough washing and removal of residue. The narrow scan of O1s, C1s, N2p, and W4f elements has been done for chemical state investigation. The major feature of the core level spectrum of C1s is a peak at around 284.6 eV, characteristic of the neutral carbon species. This peak is also ascribed to the carbon backbone of the polypyrrole. Another two components with binding energies at around 285.6 and 286.7 eV are associated with the presence of C–N and C=N or may come from contaminant or residual surfactant and environment [42]. The O1s core level peak is as expected, located at 531 eV. It can be resolved into three components, namely, as terminal oxygen (=O), the linkage oxygen (–O–), and the peak fitted around 533 eV which is assumed to come from humidity in ambience or –OH group. The photoelectron peak of the W4f region in nanocomposite showed a well-resolved double peak due to $W4f_{7/2}$ and $W4f_{5/2}$ components with $\Delta E \approx 2.1$ eV which is in good agreement with reference and revealed the presence of tungsten in W^{6+} state and oxide form in compound [41]. The peak at around 399.0 eV is attributed to the N1s which comes from polypyrrole. The spectrum deconvoluted into two major component peaks centred at 399.6 and 400.5 eV which are characteristic of pyrrolylium nitrogen's (–NH structure) and the positively charged nitrogen ($-NH^+$ (polaron)). [43, 44]. The oxidation state of W4f and O1s in WO_3 nanoparticle and WO_3-Ppy nanocomposite is shown in Figure 9. In both elements, binding energies in WO_3-Ppy nanocomposite exhibited a slight shift to the higher value compared to WO_3 nanoparticle, indicating an interaction between the WO_3 and polymer on the surface of the composite.

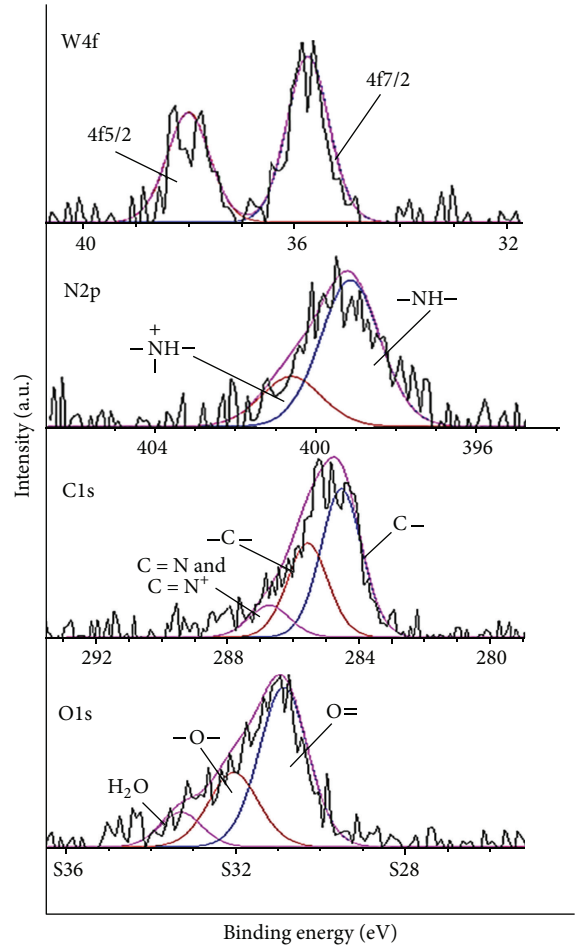

Figure 8: XPS spectra of the O1s, C1s, N2p, and W4f taken on WO_3-Ppy nanocomposite.

3.2. Optimization Parameter Reaction. The influence of metal oxide loading, AcOH/Gly mole ratio, reaction temperature, catalyst weight, and reaction time on the production of monoacetin, diacetin, and triacetin were investigated for the WO_3-polypyrrole catalyst.

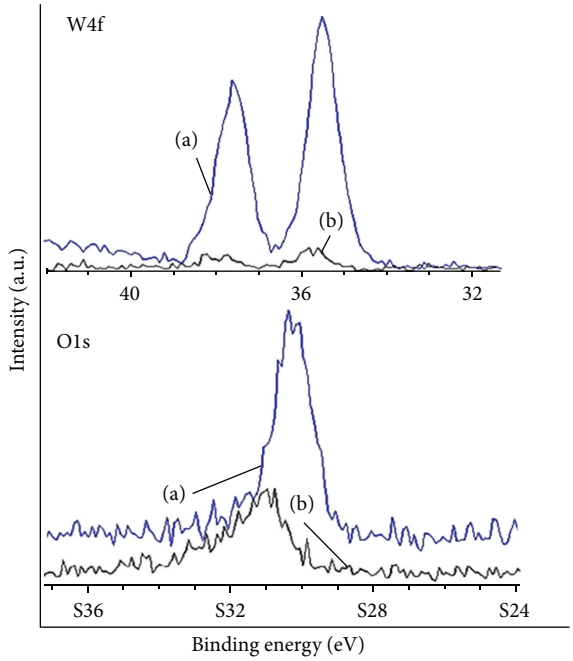

FIGURE 9: XPS spectra of the O1s and W4f in (a) WO_3 nanoparticle and (b) WO_3-Ppy nanocomposite.

3.2.1. Effect of Reaction Temperature. The temperature effect was investigated in the range of 50 to 110°C using WO_3-Ppy-20 catalyst as it exhibited maximum acidity value in NH_3-TPD analysis. The reaction temperature had a significant effect on the catalytic performance of the catalyst. The conversion increased greatly from 58.2% at 50°C to 98% at 110°C. The selectivity to monoacetin dropped sharply from 75% to about 10% while the temperature decreased from 50 to 110°C (Figure 10). Besides that, selectivity to triacetin increased drastically from about 5 to 70% at this temperature range. It was found that a higher reaction temperature favoured the conversion of glycerol and increased the selectivity towards triacetin due to the further acetylation of monoacetin, as the glycerol conversion is being completed from 50 to 110°C.

3.2.2. Effect of Reaction Time. The conversion of glycerol and the selectivity to products at different reaction times were studied using WO_3-Ppy-20 catalysts, as shown in Figure 11. The increase in conversion displayed a near linear relation with reaction time and rose from 58% to about 98% conversion within 10 h reaction time. The same trend was observed in the case of triacetin. The selectivity to triacetin increased rapidly with reaction time and hit the peak of 70% at 10 h reaction time. By contrast, the selectivity to monoacetin declined sharply after 10 h of reaction time. It is due to the monoacetin conversion to diacetin and triacetin as a result of further acetylation which is being completed from 2 to 10 hours. Along with these changes, the selectivity towards diacetin was found to increase significantly from 25% to 50% after 6 h reaction time. There was then a slight drop, reaching its primary value (25%) at 10 h of reaction time. The lower selectivity towards diacetin after a long reaction period was due to the conversion of diacetin to triacetin from further acetylation.

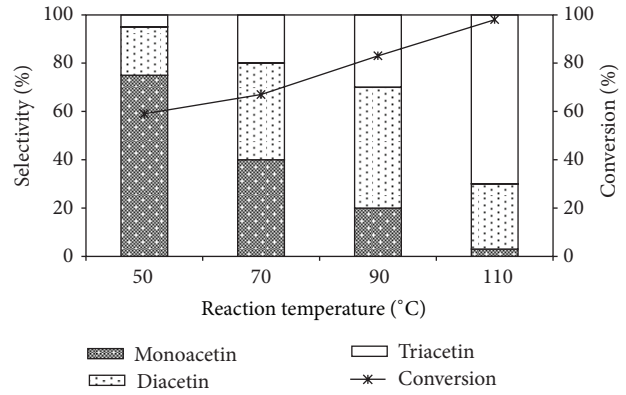

FIGURE 10: Influence of reaction temperature on glycerol acetylation over WO_3-Ppy-20 catalysts. (Reaction time: 10 h; catalyst weight: 0.4 g; AcOH/Gly mole ratio: 6.)

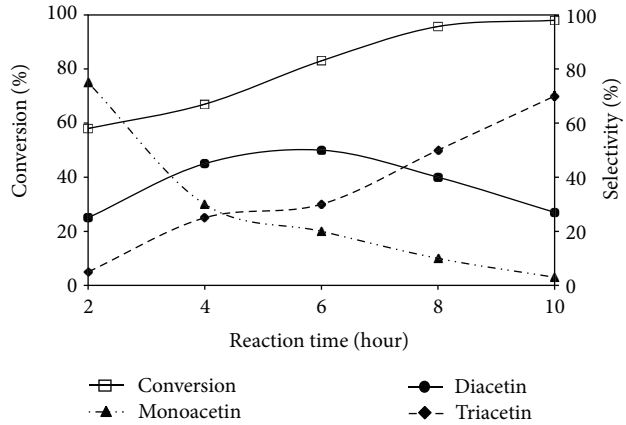

FIGURE 11: Influence of reaction time on conversion and selectivity for WO_3-Ppy-20 catalysts. (Reaction temperature: 110°C; catalyst weight: 0.4 g; AcOH/Gly mole ratio: 6.)

3.2.3. Effect of WO_3 Loading. Besides NH_3-TPD analysis to figure out the acid functionality, the effect of metal oxide loading of a catalyst on conversion and selectivity was investigated. As it is expected and examined by NH_3-TPD analysis, for acid-catalysed glycerol esterification WO_3-Ppy with 20% metal oxide loading and highest acidic performance, it showed the highest glycerol conversion and selectivity to triacetin by about 98% and 70%, respectively. As we could observe in Figure 12, catalyst with 5 wt% performed poorly in glycerol esterification with only 65% of glycerol being converted. When metal oxide was increased to 20%, glycerol conversion increased to 98%. The reaction with WO_3 as a catalyst and the blank reaction were done in the same circumstances for the sake of comparison, and the results are depicted in Figure 12.

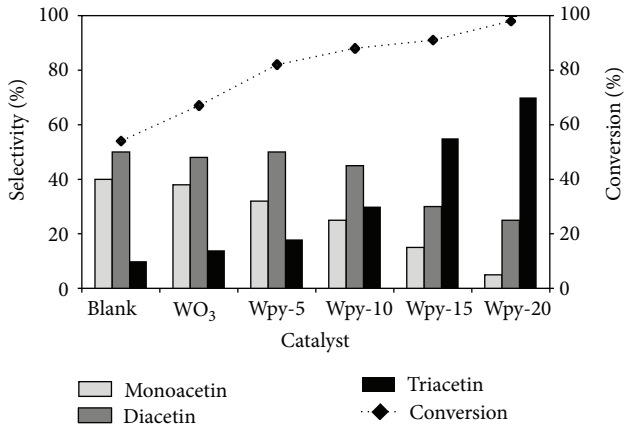

Figure 12: Influence of WO_3 loading on conversion and selectivity. (Reaction temperature: 110°C; reaction time: 10 h; catalyst weight: 0.4 g; AcOH/Gly mole ratio: 6.)

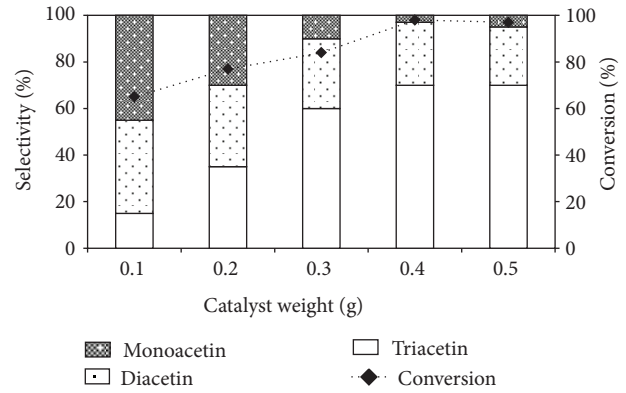

Figure 13: Influence of catalyst weight on conversion and selectivity. (Reaction temperature: 110°C; reaction time: 10 h; AcOH/Gly molar ratio: 6.)

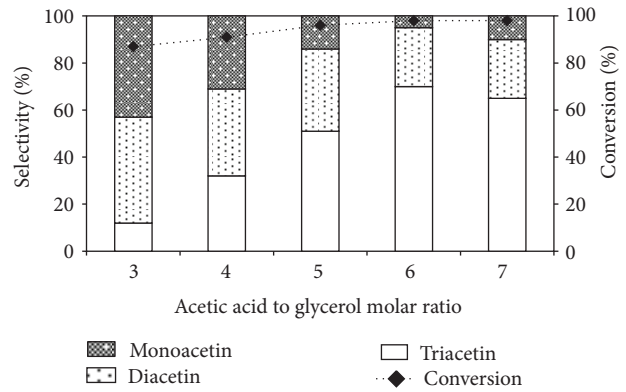

Figure 14: Influence of acetic acid to glycerol molar ratio on conversion and selectivity. (Reaction temperature: 110°C; reaction time: 10 h; catalyst weight: 0.4 g.)

3.2.4. Effect of Catalyst Weight. The effect of catalyst amount on glycerol acetylation was also investigated. The range of 0.1 to 0.5 g of catalyst was selected, while the reaction temperature was maintained at 110°C for 10 h. Figure 13 represents a slight increase in glycerol conversion with an increase in catalyst amount from 0.1 to 0.5 g. while the selectivity to monoacetin declined by catalyst amount from 45 to 5%. In contrast, in terms of triacetin, the trend was the opposite, which means, by increasing the catalyst weight, the selectivity to triacetin increased from 15% with 0.1 g catalyst to 70% with 0.5 g catalyst, confirming the consecutive type of glycerol acetylation. It is worthwhile to mention that in case of a catalyst weighing above 0.5 g, the selectivity towards products was less influenced by the catalyst amount.

3.2.5. Effect of AcOH/Gly Molar Ratio. Glycerol conversion and selectivity during acetylation of glycerol also depend on glycerol to acetic acid molar ratio. The reaction by changing the glycerol to acetic acid molar ratio from 1 : 3 to 1 : 7 was studied, and the results are shown in Figure 14. The conversion of glycerol does not vary much with a change in molar ratio. The conversion of glycerol increased with increasing acetic acid concentration in the reaction mixture, and maximum conversion was attained at a ratio of 1 : 6. The conversion was not varied above the molar ratio of 1 : 6. However, the selectivities varied with glycerol to acetic acid molar ratio. It was observed that high molar ratio of acetic acid to glycerol leads in lower selectivity values to monoacetin, which can be explained due to the high glycerol conversion which promotes the diacetin and triacetin formations. At higher acetic acid concentrations, it is expected to get more diacetin and triacetin due to the availability of more acetic acid.

4. Conclusion

The composite of WO_3 and polypyrrole provided a novel catalytic platform for a good dispersion of nanosizeed WO_3 particles and enhanced acidic properties which made a composite with a significant catalytic activity. Composite with 20% WO_3 loaded exhibited a high activity (98%) and selectivity (70%) to triacetin at 110°C and also high selectivity (75%) to monoacetin at a milder reaction condition (50°C). This study indicated that the acidity nature of polypyrrole support played a very important role in the selectivity of the composite catalyst.

Acknowledgments

The authors would like to acknowledge the Universiti Kebangsaan Malaysia (UKM) for UKM-ST-06-FRGS0147-2010 Grant and the University of Technology MARA (UiTM) for the PhD scholarship. The authors would also like to express their gratitude to CRIM and UKM for the instrument facilities provided during their study such as XPS and FESEM. Last but not least, the authors are very appreciative of the contributions and support of all the laboratory staff for this research.

References

[1] D. W. Hatchett and M. Josowicz, "Composites of intrinsically conducting polymers as sensing nanomaterials," *Chemical Reviews*, vol. 108, no. 2, pp. 746–769, 2008.

[2] P. T. Hammond, "Form and function in multilayer assembly: new applications at the nanoscale," *Advanced Materials*, vol. 16, no. 15, pp. 1271–1293, 2004.

[3] R. Gangopadhyay and A. De, "Conducting polymer nanocomposites: a brief overview," *Chemistry of Materials*, vol. 12, no. 3, pp. 608–622, 2000.

[4] M. Michel, F. Ettingshausen, F. Scheiba, A. Wolz, and C. Roth, "Using layer-by-layer assembly of polyaniline fibers in the fast preparation of high performance fuel cell nanostructured membrane electrodes," *Physical Chemistry Chemical Physics*, vol. 10, no. 25, pp. 3796–3801, 2008.

[5] A. N. Grace and K. Pandian, "Pt, Pt–Pd and Pt–Pd/Ru nanoparticles entrapped polyaniline electrodes—a potent electrocatalyst towards the oxidation of glycerol," *Electrochemistry Communications*, vol. 8, no. 8, pp. 1340–1348, 2006.

[6] H. J. Salavagione, C. Sanchís, and E. Morallón, "Friendly conditions synthesis of platinum nanoparticles supported on a conducting polymer: methanol electrooxidation," *Journal of Physical Chemistry C*, vol. 111, no. 33, pp. 12454–12460, 2007.

[7] Y. Xian, Y. Hu, F. Liu, Y. Xian, H. Wang, and L. Jin, "Glucose biosensor based on Au nanoparticles-conductive polyaniline nanocomposite," *Biosensors and Bioelectronics*, vol. 21, no. 10, pp. 1996–2000, 2006.

[8] J. M. Kinyanjui, N. R. Wijeratne, J. Hanks, and D. W. Hatchett, "Chemical and electrochemical synthesis of polyaniline/platinum composites," *Electrochimica Acta*, vol. 51, no. 14, pp. 2825–2835, 2006.

[9] Z. A. Hu, L. J. Ren, X. J. Feng et al., "Platinum-modified polyaniline/polysulfone composite film electrodes and their electrocatalytic activity for methanol oxidation," *Electrochemistry Communications*, vol. 9, no. 1, pp. 97–102, 2007.

[10] S. Domínguez-Domínguez, J. Arias-Pardilla, A. Berenguer-Murcia, E. Morallón, and D. Cazorla-Amorós, "Electrochemical deposition of platinum nanoparticles on different carbon supports and conducting polymers," *Journal of Applied Electrochemistry*, vol. 38, no. 2, pp. 259–268, 2008.

[11] F. J. Liu, L. M. Huang, T. C. Wen, K. C. Yin, J. S. Hung, and A. Gopalan, "Composite electrodes consisting of platinum particles and polyaniline nanowires as electrocatalysts for methanol oxidation," *Polymer Composites*, vol. 28, no. 5, pp. 650–656, 2007.

[12] M. Hasik, A. Drelinkiewicz, M. Choczyński, S. Quillard, and A. Proń, "Polyaniline containing palladium—new conjugated polymer supported catalysts," *Synthetic Metals*, vol. 84, no. 1–3, pp. 93–94, 1997.

[13] S. W. Huang, K. G. Neoh, C. W. Shih et al., "Synthesis, characterization and catalytic properties of palladium-containing electroactive polymers," *Synthetic Metals*, vol. 96, no. 2, pp. 117–122, 1998.

[14] J. A. Smith, M. Josowicz, and J. Janata, "Gold-polyaniline composite—part I: moving electrochemical interface," *Physical Chemistry Chemical Physics*, vol. 7, no. 20, pp. 3614–3618, 2005.

[15] J. A. Smith, M. Josowicz, M. Engelhard, D. R. Baer, and J. Janata, "Gold-polyaniline composites—part II: effects of nanometer sized particles," *Physical Chemistry Chemical Physics*, vol. 7, no. 20, pp. 3619–3625, 2005.

[16] B. M. Weckhuysen and D. E. Keller, "Chemistry, spectroscopy and the role of supported vanadium oxides in heterogeneous catalysis," *Catalysis Today*, vol. 78, no. 1–4, pp. 25–46, 2003.

[17] W. Turek, Edyta-Stochmal-Pomarzańska, A. Proń, and J. Haber, "Propylene oxidation over poly(azomethines) doped with heteropolyacids," *Journal of Catalysis*, vol. 189, no. 2, pp. 297–313, 2000.

[18] W. Turek, M. Lapkowski, A. Stolarczyk, and J. Debiec, "EPR and XPS measurements of polymeric catalysts doped with hereopolyacids in oxygen adsorption studies," *Applied Surface Science*, vol. 252, no. 3, pp. 801–806, 2005.

[19] J. Poźniczek, I. Kulszewicz-Bajer, M. Zagórska et al., "$H_3PMo_{12}O_{40}$-doped polyacetylene as a catalyst for ethyl alcohol conversion," *Journal of Catalysis*, vol. 132, no. 2, pp. 311–318, 1991.

[20] J. Y. Lee, Y. Liao, R. Nagahata, and S. Horiuchi, "Effect of metal nanoparticles on thermal stabilization of polymer/metal nanocomposites prepared by a one-step dry process," *Polymer*, vol. 47, no. 23, pp. 7970–7979, 2006.

[21] M. Sangermano, Y. Yagci, and G. Rizza, "In situ synthesis of silver-epoxy nanocomposites by photoinduced electron transfer and cationic polymerization processes," *Macromolecules*, vol. 40, no. 25, pp. 8827–8829, 2007.

[22] K. I. H. Nabeshima, JP Patent 276787, 1995.

[23] P. Hofmann, DE Patent 3512497, 1985.

[24] T. H. S. Nomura, JP Patent 203429, 1995.

[25] B. Nebel, M. Mittelbach, and G. Uray, "Determination of the composition of acetylglycerol mixtures by 1H NMR followed by GC investigation," *Analytical Chemistry*, vol. 80, no. 22, pp. 8712–8716, 2008.

[26] T. Watanabe, M. Sugiura, M. Sato, N. Yamada, and K. Nakanishi, "Diacylglycerol production in a packed bed bioreactor," *Process Biochemistry*, vol. 40, no. 2, pp. 637–643, 2005.

[27] A. O. Y. Taguchi, Y. Ikeda, K. Fujita, and T. Masuda, JP Patent 298099, 2000.

[28] J. Sohn, "Progress in solid superacid catalyst," *Journal of Industrial and Engineering Chemistry*, vol. 10, p. 1, 2004.

[29] T. K. Cheung, J. L. D'itri, F. C. Lange, and B. C. Gates, "Neopentane cracking catalyzed by iron- and manganese-promoted sulfated zirconia," *Catalysis Letters*, vol. 31, no. 2-3, pp. 153–163, 1995.

[30] A. A. Kiss, F. Omota, A. C. Dimian, and G. Rothenberg, "The heterogeneous advantage: biodiesel by catalytic reactive distillation," *Topics in Catalysis*, vol. 40, no. 1–4, pp. 141–150, 2006.

[31] M. Hino and K. Arata, "Synthesis of solid superacid of tungsten oxide supported on zirconia and its catalytic action for reactions of butane and pentane," *Journal of the Chemical Society, Chemical Communications*, no. 18, pp. 1259–1260, 1988.

[32] N. Laosiripojana, W. Kiatkittipong, W. Sutthisripok, and S. Assabumrungrat, "Synthesis of methyl esters from relevant palm products in near-critical methanol with modified-zirconia catalysts," *Bioresource Technology*, vol. 101, no. 21, pp. 8416–8423, 2010.

[33] K. N. Rao, A. Sridhar, A. F. Lee, S. J. Tavener, N. A. Young, and K. Wilson, "Zirconium phosphate supported tungsten oxide solid acid catalysts for the esterification of palmitic acid," *Green Chemistry*, vol. 8, no. 9, pp. 790–797, 2006.

[34] H. S. Ghaziaskar, A. Daneshfar, and L. Calvo, "Continuous esterification or dehydration in supercritical carbon dioxide," *Green Chemistry*, vol. 8, no. 6, pp. 576–581, 2006.

[35] J. Zhu, S. Wei, L. Zhang et al., "Conductive polypyrrole/tungsten oxide metacomposites with negative permittivity," *Journal of Physical Chemistry C*, vol. 114, no. 39, pp. 16335–16342, 2010.

[36] X. Yang and Y. Lu, "Preparation of polypyrrole-coated silver nanoparticles by one-step UV-induced polymerization," *Materials Letters*, vol. 59, no. 19-20, pp. 2484–2487, 2005.

[37] C. Martin, I. Martin, V. Rives et al., "Physicochemical characterization of WO_3/ZrO_2 and WO_3/Nb_2O_5 catalysts and their photoactivity for 4-nitrophenol photooxidation in aqueous dispersion," *Journal of Materials Science*, vol. 32, no. 22, pp. 6039–6047, 1997.

[38] A. Corma, V. Fornés, M. I. Juan-Rajadell, and J. M. L. Nieto, "Influence of preparation conditions on the structure and catalytic properties of SO_4^{2-}/ZrO_2 superacid catalysts," *Applied Catalysis A*, vol. 116, no. 1-2, pp. 151–163, 1994.

[39] L. Chen, J. Li, M. Ge, L. Ma, and H. Chang, "Mechanism of selective catalytic reduction of NO_x with NH_3 over CeO_2-WO_3 catalysts," *Chinese Journal of Catalysis*, vol. 32, no. 5, pp. 836–841, 2011.

[40] C. Hess, "Nanostructured vanadium oxide model catalysts for selective oxidation reactions," *ChemPhysChem*, vol. 10, no. 2, pp. 319–326, 2009.

[41] N. Asim, S. Radiman, and M. A. Yarmo, "Preparation of WO_3 nanoparticles using cetyl trimethyl ammonium bromide supermolecular template," *The American Journal of Applied Sciences*, vol. 6, no. 7, pp. 1424–1428, 2009.

[42] P. Lisboa, D. Gilliland, G. Ceccone, A. Valsesia, and F. Rossi, "Surface functionalisation of polypyrrole films using UV light induced radical activation," *Applied Surface Science*, vol. 252, no. 13, pp. 4397–4401, 2006.

[43] R. Rajagopalan and J. O. Iroh, "Characterization of polyaniline-polypyrrole composite coatings on low carbon steel: a XPS and infrared spectroscopy study," *Applied Surface Science*, vol. 218, no. 1–4, pp. 58–69, 2003.

[44] J. Dejeu, A. E. Taouil, P. Rougeot, S. Lakard, F. Lallemand, and B. Lakard, "Morphological and adhesive properties of polypyrrole films synthesized by sonoelectrochemical technique," *Synthetic Metals*, vol. 160, no. 23-24, pp. 2540–2545, 2010.